Usage Report for Fiscal Year 2024

Project Title:

Ab-initio structure search orientated design of room-temperature superconductors in ternary hydrides

Name:
○Yanming MA (1), Yu XIE (1), and Toshiaki IITAKA (2)
Laboratory at RIKEN:
(1) Jilin University, Collage of Physics
(2) RIKEN Center for Computational Science, Discrete Event Simulation Research Team

1. Background and purpose of the project, relationship of the project with other projects

The experimental study has shown that $LaBeH_8$ exhibits the highest T_c of 110 K at ~80 GPa. setting a milestone of the lowest-ever pressure for superconducting hydrides with T_c above the liquid nitrogen temperature of 77 K. Moreover, many theoretical studies tried to lower dynamically stable pressures for the compounds isostructural to $LaBeH_8$. It is natural to wonder if the thermodynamically stable pressure of this $LaBeH_8$-like prototype structure could be further lowered via doping additional metal elements that introduce considerable entropy at typically realistic temperature, such as ~2000 K, for synthesizing high-temperature superconducting hydrides.

Niobium (Nb), with the highest T_c under ambient pressure, has sparked significant research interest in its hydrides. At low hydrogen content, hydrogen randomly dissolves in Nb at tetrahedral interstitial tetrahedral (*T*) sites, resulting in the formation of non-stoichiometric NbH_x ($0 < x < 0.7$), which exhibits T_c up to 9.4 K. In the concentration range of $0.7 < x < 1.1$, the Nb sublattice of NbH_x undergoes a structural transformation from body-centered cubic (*bcc*) to face-centered orthorhombic, accompanied by several phase transitions resulting from the ordering of vacancies in the hydrogen sublattice at low temperatures. However, superconductivity has not been observed in these structures. Recently, first-principles calculations have predicted that Nb hydrides exhibit enhanced superconductivity under pressures, notably body-centered tetragonal (*bct*) NbH_4 and orthorhombic NbH_{11} with T_cs of 38-47 K and 117-137 K at 300 GPa, respectively. Consequently, a series of Nb hydrides with increased hydrogen content has been successfully synthesized under elevated pressures[45]. In addition to distorted *bcc* NbH_3 and hexagonal close-packed $NbH_{2.5}$, non-stoichiometric face-centered cubic (*fcc*) $NbH_{2.5-3}$ was also proposed in this work. Most recently, an experimental work claimed the discovery of *fcc* NbH_3 and reported the anticipated superconductivity with a T_c of 42 K. Due to the occurrence of non-stoichiometric ratios in Nb hydrides at moderate pressures and their relatively low hydrogen concentration, which facilitates quantitative analysis through lattice volume expansion, this superconducting system could be regarded as an ideal candidate for the exploration of the relationship between hydrogen vacancies and the superconductivity of hydride under high pressure

2. Specific usage status of the system and calculation method

In the first work, the energetic calculations in our study were carried out by employing the Vienna *ab initio* simulation package (VASP), which is based on density functional theory within the generalized gradient approximation (GGA) in the form of the Perdew-Burke-Ernzerh (PBE) of exchange-correlation functional. The electron-ion interaction is

described by all-electron projector-augmented wave (PAW)エラー! 参照元が見つかりません。 method, wherein $5s^25p^65d^16s^2$, $4s^24p^64d^15s^2$, $4f^15s^25p^65d^16s^2$, $5f^16s^26p^66d^17s^2$, $1s^22s^2$ and $1s^1$ serve as the valence electrons for La, Ce, Y, Th, Be, and H, respectively. The kinetic cutoff energy for plane-wave basis set with 900 eV and Monkhorst-Pack k meshes with a resolution of 0.18 $Å^{-1}$ are utilized to ensure the enthalpy converges well. The formation enthalpy of all alloy structures against the decomposition paths are calculated by Pymatgen.

The lattice dynamics and electron-phonon coupling of the stable structures are calculated within the framework of density functional perturbation theory through the Quantum-ESPRESSO code, where PAW pseudopotentials were adopted with a kinetic energy cutoff of 80 Ry. Self-consistent electron density and EPC were calculated by employing 16 × 16 × 16 *k*-point meshes and 4 × 4 × 4 *q*-point meshes for *Pmmm* phase, 20 × 20 × 16 and 5 × 5 × 4 for *P*4/*mmm* phase, 12 × 16 × 16 and 3 × 4 × 4 for *P*1 phase. The superconducting gap and T_c value were calculated by numerically solving the isotropic Eliashberg equations with the ELK code.

In the second work, structures of $NbH_{4-\delta}$ with vacancy concentration δ ranging from 0.22 to 0.75 were generated in a 2×2×2 supercell of *sc* NbH4 containing 160 atoms by Python Materials Genomics (pymatgen) analysis code and the alloy theoretic automated toolkit (ATAT), and then ordered based on an electrostatic energy criterion via the pymatgen. Nb and H were assigned "idealized" charges based on their valence states, i.e., +4 for Nb and -1 for H, respectively. For each vacancy concentration, 10-50 structures with the lowest electrostatic energy were selected for relaxations. To assess the possible interaction between the vacancies, the differences in enthalpy for various-sized quasi-random NbH3.50 supercells are calculated to be less than 1 meV/atom.

The structural relaxations and electronic properties calculations were performed using Density functional theory (DFT) within the Perdew–Burke–Ernzerhof9 generalized gradient approximation exchange-correlation functional, as implemented in the VASP code. The all-electron projector-augmented wave11 method was employed, wherein $4s^24p^64d^45s^1$ and $1s^1$ serve as the valence electrons for Nb and H, respectively. Plane-wave kinetic energy cutoff was set to 800 eV, and Monkhorst–Pack k-meshes12 with a grid spacing of 2π×0.03 $Å^{-1}$ was utilized to ensure the enthalpy converges well. The harmonic phonon calculations were carried out using the supercell approach and finite displacement method implemented in the PHONOPY code13 and the VASP code. The electron-phonon coupling (EPC) constant was calculated within the density functional perturbation theory as carried out in the Quantum ESPRESSO package. Ultra-soft pseudopotentials were used with a kinetic energy cutoff of 80 Ry. To calculate the EPC in $NbH_{4-\delta}$, 6×6×6 q mesh was utilized. The Gaussian broadening is 0.02 Ry for all structures.

3. Result

3.1 En route to lower synthesis pressure of superconducting hydrides via alloying substitution of guest La atoms in $LaBeH_8$

We begin our first-principles simulations on the experimentally synthesized $LaBeH_8$-type structure by substituting La atoms with three different elements with considering configurational entropy at 2000 K. The results show that the combinations of La/Th, La/Ce, and Ce/Th for quasi-binary alloy hydrides can maintain thermodynamically stable within megabar pressure at 2000 K. For example, (La, Th)BeH_8 with an equal mole of La and Th is thermodynamically stable at a much lower pressure of 91 GPa than ~110 GPa as for $LaBeH_8$ at 2000 K in the top panel of Fig. 1 (a). Additionally, (La, Ce)BeH_8 also can maintain thermodynamic stability under pressures of 99 GPa at 2000 K, which motivated us to

investigate quasi-ternary and quasi-quaternary alloy hydrides. As a consequence, (La, Ce, Th)BeH_8 are computed to be thermodynamically stable above 87 GPa at 2000 K, and the quasi-quaternary alloy hydride (La, Y, Ce, Th)BeH_8 exhibits thermodynamic stability above 123 GPa at 2000 K in the present study [The top panel of Fig. 1 (a)]. The complete calculation results for free energies with respect to pressure of other alloys are described in Appendix B. Our findings demonstrate that configurational entropy drives the multi-elemental alloys to maintain thermodynamic stability at typical experimental temperatures (2000 K) within megabar pressure.

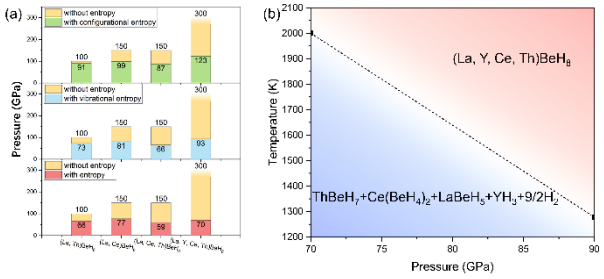

FIG. 1. (a) Comparison of the lowest thermodynamically stable pressures in alloy hydrides with or without different entropy effects. Yellow bars represent the lowest thermodynamically stable pressures at 0 K, while green, blue and red bars correspond to the lowest thermodynamically stable pressures at 2000 K, when configurational, vibrational entropy or both are included, respectively. It is noted that (La, Y, Ce, Th)BeH_8 is thermodynamically unstable even at 300 GPa. (b) Pressure-temperature phase diagram of (La, Y, Ce, Th)BeH_8 by considering the contribution of configurational and vibrational entropy.

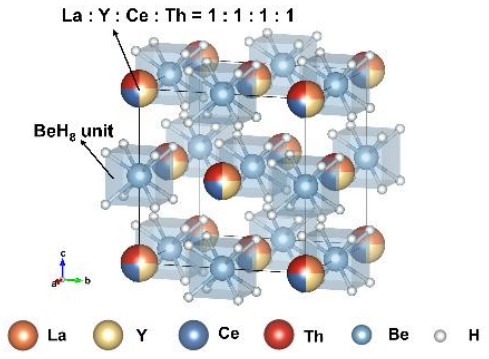

FIG. 2. Alloy structure of (La, Y, Ce, Th)BeH_8. Orange, yellow, dark blue, red, dusty blue, and grey spheres represent La, Y, Ce, Th, Be, and H atoms, respectively.

The hydrides mentioned above were considered as a superconducting alloy composed of a distorted BeH_8 sublattice and randomly substituted metal sublattice as shown in typical (La, Y, Ce, Th)BeH_8 (Fig. 2) akin to the high-entropy ceramics. To examine the influence of the cell size and configurational disorder on energy stability as reported in (Y, Sr)H_{22}, in this study, we took (La, Y, Ce, Th)BeH_8 as a representative example to perform the quasi-random structure (SQS) simulations, the best way to mimic a substitutional alloy structure, to check if the crystal structure model with the simulated cell of 40 atoms is accurate enough to describe the system, before any further analysis. We thus carried out structural relaxations at a representative pressure of 100 GPa and found that the energy variations among these quasi-random structures (the unit cells of 40 and 160 atoms) were within an energy deviation of ~2 meV/atom (Fig. 3). This indicates that cell size does not apparently affect the study of the structure of (La, Y, Ce, Th)BeH_8.

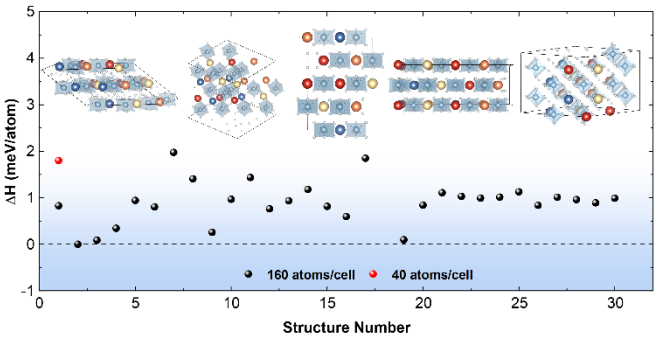

FIG. 3. The calculated enthalpy of (La, Y, Ce, Th)BeH_8 with different assignments of La, Y, Ce, and Th atoms to SQS site classes at 100 GPa, where the SQS supercells with 160 atoms display five distinct typical lattice configurations.

It is known that configurational entropy has been long believed to play a key role in the stability of multi-elemental alloy. However, in addition to configurational entropy, vibrational entropy should be considered for a comprehensive study of the stability of the alloy system at high temperatures. We then compared the effect of configurational and vibrational entropy on the thermodynamic stability in the aforementioned alloy hydrides. The results show that the thermodynamically stable pressures

considering vibrational entropy are several tens GPa lower than those considering configurational entropy in middle panel of Fig. 1 (a). Motivated by these unexpected results, we further estimated the thermodynamically stable pressures of these predicted alloy hydrides by considering both vibrational and configurational entropy, as shown in bottom panel of Fig. 1 (a), such as (La, Th)BeH_8 (66 GPa at 2000 K) and (La, Ce)BeH_8 (77 GPa at 2000 K). Regarding (La, Ce, Th)BeH_8 and (La, Y, Ce, Th)BeH_8, they can maintain thermodynamically stable above 60 and 70 GPa, respectively, at 2000 K. These results indicate that the contribution of vibrational entropy to thermodynamic stability for alloy cannot be overlooked at high temperatures. More results are shown in Fig. 4. Moreover, we also provide the pressure-temperature phase diagram of (La, Y, Ce, Th)BeH_8 [Fig. 1(b)], which indicates that the entropy effect can indeed optimize the stable pressures of multi-component alloys with increasing temperature.

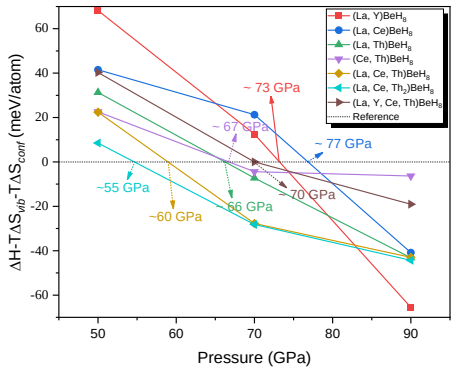

FIG. 4. Calculated Gibbs free energy for (La,Y)BeH_8, (La,Ce)BeH_8, (La,Th)BeH_8, (Ce,Th)BeH_8, (La,Ce,Th)BeH_8 (La,Ce,Th_2)BeH_8 and (La,Y,Ce,Th) BeH_8 as a function of pressure considering the contribution of configurational entropy (ΔS_{conf}) and vibrational entropy (ΔS_{vib}) at pressure-temperature conditions of 50-90 GPa and 2000 K.

Finally, we evaluate the T_cs by numerically solving the Migdal-Eliashberg equations directly, and the obtained T_c values, along with the EPC parameter λ and the phonon frequency logarithmic average ω_{log} for these alloy hydrides, are shown in Table 1. (La, Ce)BeH_8, (La, Th)BeH_8, and (La, Ce, Th)BeH_8 exhibit T_c values of 58-66 at 77 GPa, 83-92 K at 66 GPa, and 49-57 K at 60 GPa by using typical coulomb pseudopotential parameters μ^* of 0.13-0.10. Notably, the T_c of (La, Y, Ce, Th)BeH_8 is estimated to range from 87 to 98 K (μ^* = 0.13 - 0.10) at 70 GPa, exceeding the liquid nitrogen temperature of 77 K. The further results revealed that T_c and EPC parameter λ increase with decreasing pressure, while ω_{log} values show the opposite trend.

TABLE 1. The calculated EPC constant (λ), phonon frequency logarithmic average (ω_{log}), and superconducting critical temperature T_c (μ^* = 0.13 and 0.1) by numerically solving the Eliashberg equations for various alloy structures under given pressures. For each alloy structure, the second pressure point is the lowest thermodynamic stability pressure, and the third pressure point is the lowest kinetic stability pressure.

Formulas	P(GPa)	λ	ω_{log}(K)	T_c (EA) (K)
(La, Y)BeH_8	100	1.88	986	188-195
	73	2.20	847	192-201
	50	3.18	621	204-213
(La, Ce)BeH_8	100	0.74	1226	53-65
	77	0.81	1136	58-66
	17	1.58	620	96-104
(La, Th)BeH_8	100	0.83	1277	66-81
	66	0.94	1148	83-92
	10	1.89	654	121-127
(Ce, Th)BeH_8	100	0.50	1242	14-22
	67	0.55	1086	13-19
	17	1.04	519	44-50
(La, Ce, Th)BeH_8	100	0.61	1281	23-32
	60	0.77	1061	49-57
	30	1.12	759	66-76
(La, Ce, Th_2)BeH_8	100	0.56	1259	20-28
	55	0.75	1057	48-55
	20	1.06	730	63-73
(La, Y, Ce, Th)BeH_8	100	0.89	1173	73-84
	70	1.04	1027	87-98
	32	1.68	635	104-112

3.2 Hydrogen-Vacancy-Induced Stable Superconducting Niobium Hydride at High Pressure

In this work, we report the synthesis of non-stoichiometric $NbH_{4-\delta}$ with δ values ranging from 0.23 to 0.51. *In-situ* high-pressure x-ray diffraction (XRD) experiments reveal that the Nb sublattice adopts an *fcc* structure. Combining multiple rounds of experimental equation of state (EOS) and extensive first-principles computational simulations, we provide clear evidence for the presence of hydrogen vacancies within the pressure range of 113-175 GPa.

To comprehend this observed non-stoichiometric $NbH_{4-\delta}$ structure, we therefore construct a theoretical structural model based on the experimental hydrogen content of 3.49-3.77. Considering the *fcc* metal

sublattice of *sc* NbH_4 consistent with experimental results, we randomly removed the appropriate amount of hydrogen atoms in the 2×2×2 supercell of *sc* NbH_4 containing 128 hydrogen atoms, to simulate the hydrogen vacancies. By screening millions of randomly generated structures, we identified ~450 relatively low-energy configurations with varying hydrogen concentrations (δ~0.22-0.75) at 170 GPa.

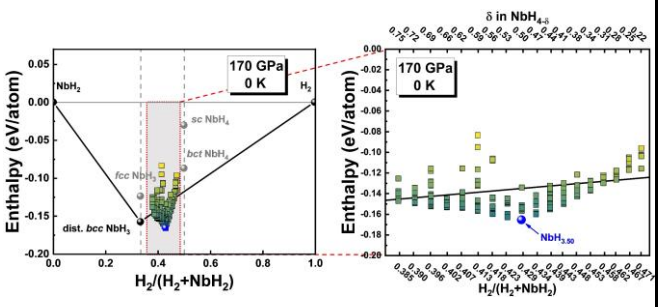

Figure 1. Calculated convex hull of the Nb-H binary system and formation enthalpy of NbH3.50 at 170 GPa. The black and gray circles represent thermodynamically stable and unstable stoichiometric Nb hydrides. The right-hand figure is an enlarged view of the red rectangle on the left, where the square dots represent the non-stoichiometric NbH4-δ with δ ranging from 0.22

As shown in Figure 1, a substantial number of structures with hydrogen content in the range of 3.25-3.78 exhibit a distinct energetic advantage relative to the thermodynamically stable distorted *bcc* NbH_3 and H_2 at zero temperature. Moreover, we performed extensive crystal structure searches for a range of stoichiometries across all symmetries; however, no additional simple stable stoichiometry was identified between NH_3 and NbH_4 in the current calculations. To investigate the low-energy structures, we further simulated various configurations with hydrogen vacancies in *T* sites. In a larger 3×3×3 supercell (540 atoms), 100 different $NbH_{3.50}$ structures, as typical representatives of non-stoichiometric $NbH_{4-\delta}$, were constructed by randomly removing a quarter of the hydrogen atoms in *T* sites. The energy differences among a large number of configurations for the typical concentration of $NbH_{3.50}$ are virtually indistinguishable (Figure 2a), suggesting a strong tendency for hydrogen vacancies to be disordered.

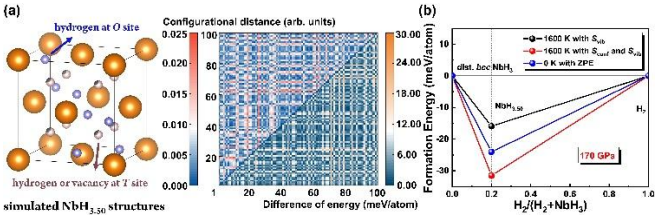

Figure 2. Configurational and energetic differences among 100 distinct NbH3.50 structures and the effect of entropy on the stability of NbH3.50 at 170 GPa. (a) The 100 different NbH3.50 structures were constructed by randomly removing the tetrahedral hydrogen atom in a 3×3×3 supercell (540 atoms) of the conventional unit cell of the sc NbH_4 structure. The corresponding schematic of the crystal structure is shown in the left panel. The calculated configurational distance matrix and energetic difference matrix for these 100 structures are mapped to the upper-left and lower-right triangular portions of the symmetric matrix in the right panel, respectively. The color scale of the matrix elements indicates the energy or configurational differences between the associated pairs of structures. (b) The blue symbols represent the enthalpy of representative NbH3.50 at 0 K, considering the zero-point energy (ZPE). The formation energy including vibrational entropy at 1600 K is shown in the black symbol, while the red one accounts for both configurational and vibrational entropy at 1600 K.

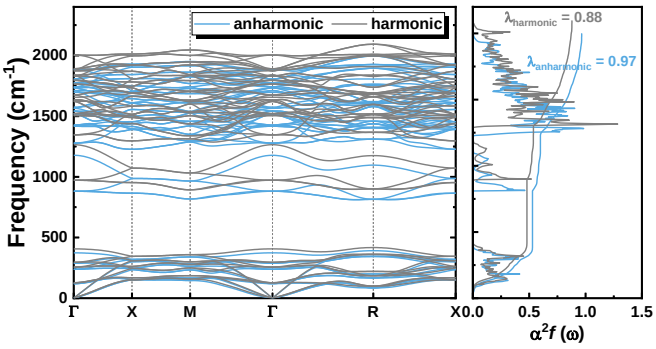

Figure 3. Phonon spectra with the harmonic and anharmonic levels of NbH3.50 at 170 GPa. The gray and blue lines on the left panel represent the harmonic and anharmonic phonon spectra. The right panel shows the α2F(ω) function together with the integrated electron-phonon coupling constant .

Thermodynamically, the Gibbs energy reaches a minimum at a specific vacancy concentration, due to the balance between the overall vacancy formation enthalpy, vibrational entropy, and configurational entropy of vacancies. We select ordered *Pn*-3*m* structured $NbH_{3.50}$ as an approximation to reevaluate the formation energy of non-stoichiometric $NbH_{4-\delta}$ at 1600 K, incorporating zero-point energy,

configurational entropy, and vibrational entropy (Figure 1b). Interestingly, configurational disorder significantly contributes to the stabilization of $NbH_{3.50}$, while vibrational contribution increases its energy. Beyond thermodynamic stability, the absence of negative phonon frequencies in phonon dispersion of *Pn*-3*m* $NbH_{3.50}$ confirms its dynamic stability (Figure 3). In contrast, stoichiometric *fcc* NbH_3 and *sc* NbH_4, both with an *fcc* Nb sublattice, are dynamically unstable, even when accounting for anharmonic and temperature effects (Figure 4), thus completely ruling out the possibility of stoichiometric compositions.

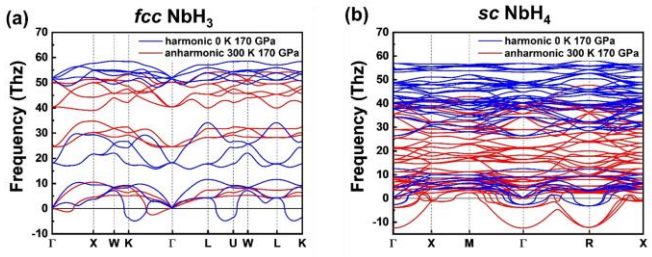

Figure 4. Calculated phonon dispersion curves of fcc NbH3 and sc NbH4 at 170 GPa. Phonon spectra of fcc NbH3 and sc NbH4 are shown in (a) and (b). Harmonic phonon dispersion curves computed with density functional perturbation theory (DFPT) at 0 K and anharmonic phonon dispersion curves computed with temperature-dependent effective potentials (TDEP) at 300 K of fcc NbH3 and sc NbH4 are distinguished by blue and red lines, respectively.

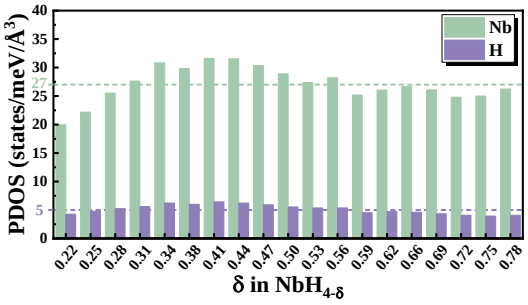

Figure 5. The projected electronic density of states (PDOS) at the Fermi level in different hydrogen vacancy concentrations. The dashed lines represent the average value of the PDOS at the Fermi level for Nb (green) and H (purple), respectively.

To investigate the electronic properties and superconductivity of $NbH_{4-\delta}$, we examined the DOS at the Fermi level across structures with varying vacancy contents (Figure 5). The DOS at the Fermi level is predominantly governed by *d* electrons of Nb and *s* electrons of H, with Nb making a more significant contribution. Considering the quite similar DOS across all simulated vacancy concentrations, especially in the experimentally synthesized vacancy range from 0.23 to 0.51, further simulations were performed on the representative structure $NbH_{3.50}$.

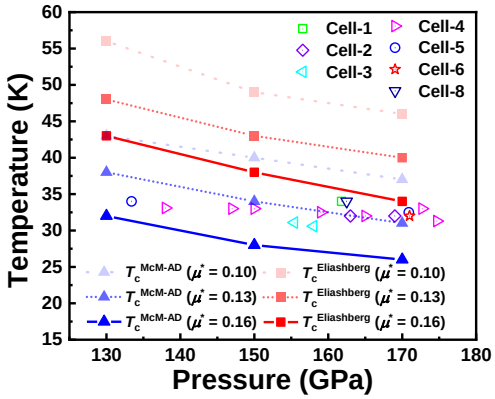

Figure 6. Calculated Tc of $NbH_{3.50}$. Distinct colors of hollow points distinguish the experimental data originating from different cells. Calculated Tc values obtained from McMillan-Allen-Dynes (McM-AD) and Eliashberg equations as a function of pressure are characterized by blue and red solid points, respectively. The solid (μ* = 0.16), short dot (μ* = 0.13), and dot (μ* = 0.10) lines represent different Coulomb shielding constants.

As shown in Figure 6, the T_c of $NbH_{3.50}$ and its decreasing trend with increasing pressure were reproduced by solving the McMillan-Allen-Dynes (37-26 K at 170 GPa, μ^* = 0.10-0.16) and Eliashberg formulations (46-34 K at 170 GPa, μ^* = 0.10-0.16). The discrepancy between experimental and calculated T_c values might stem from variations in hydrogen content between simulated $NbH_{3.50}$ and synthesized $NbH_{4-\delta}$, as well as the unaccounted anharmonic effects and anisotropy in the electron-phonon coupling calculations. For instance, the calculated T_c of $NbH_{3.50}$ increases from 40 K to 44 K (μ^* = 0.13) at 170 GPa by solving the isotropic Migdal-Eliashberg equations with anharmonic effects (Figure 3). Notably, different from the hydrogen-dominant strong electron-phonon coupling (EPC) in MH_6, MH_9, or MH_{10} superhydrides (*M* represent

metal atoms), which mainly arise from vibration modes of hydrogen cages, the vibrations of Nb in the low-frequency zone (Figure 7) make a significant contribution (55%) to the EPC constant λ. Meanwhile, the vibrations of H in the middle-frequency and high-frequency zones also make a non-negligible contribution to the λ (45%), despite the lack of noticeable H-H bonds (the H-H distances is 1.34-1.68 Å). This characteristic sets it apart from metal-dominated superconductors like PdH or PtH (the H-H distance beyond 2.5 Å)

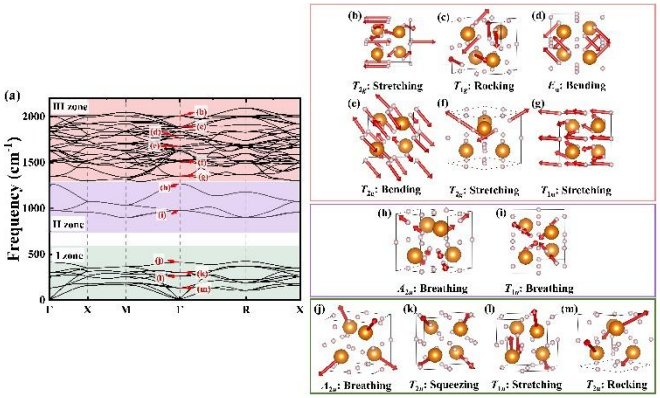

Figure 7. Phonon band structures (a) and typical vibration modes (b-m) of NbH3.50 at 170 GPa. The H–H interaction in NbH3.50 predominantly exhibits bending, stretching, and rocking rotational vibration modes (b-g) in the high-frequency region, as well as tetrahedral breathing vibrations (h-i) in the mid-frequency range, at point. Similarly, the Nb lattice also undergoes tetrahedral breathing vibrations (j) in the low-frequency region. Additionally, the squeezing, stretching, and rocking motions (k-m) of the Nb lattice together contribute to the large electron-phonon coupling (EPC) in NbH3.50.

4. Conclusion

We combine La, Y, Ce, and Th elements in various ratios at the La sites within the parent structure $LaBeH_8$ to form alloy structures. To assess the realistic conditions of experimental synthesis, we estimated the stability of these predicted alloy hydrides, by taking into account the important contribution of configurational and vibrational entropy to Gibbs free energy at high temperatures. (La, Ce)BeH_8, (La, Th)BeH_8, (La, Ce, Th)BeH_8, and (La, Y, Ce, Th)BeH_8 can maintain thermodynamic stability above 77, 66, 60, and 70 GPa at 2000 K, respectively. Our in-depth analysis indicates that vibrational entropy plays a much more significant role than configurational entropy in stabilizing these alloy hydrides as unexpected, where configurational entropy has been widely regarded as a pivotal factor in the stability of multi-elemental alloy. Furthermore, EPC calculations reveal that all alloy hydrides have the potential to become superconductors within pressures of tens of GPa, especially for (La, Y, Ce, Th)BeH_8 with T_c of 87-98 K at 70 GPa. The simulations also suggest several hydrogen-based alloys with high T_cs above the liquid nitrogen temperature of 77 K at moderate pressures. Our findings shed light on the design and discovery of high-temperature superconductivity via multi-elemental alloy hydrides at near-ambient pressure conditions.

In the second work, We have found cubic non-stoichiometric superconducting $NbH_{4-\delta}$ with prominent hydrogen vacancies under high pressure. Within the pressure range of 133-175 GPa in electrical experiments, the data exhibits a slight increase in T_c with decreasing pressure, reaching a maximum value of 34 K. Further simulations suggested that hydrogen vacancies play a critical role in stabilizing such superconducting hydride under high pressure. These results offer a unique platform for investigating the hydrogen vacancies, stability, and superconductivity among non-stoichiometric superconducting hydrides under high pressures.

5. Schedule and prospect for the future

We have been HOKUSAI general users and wish to continue using the system. During the last fiscal year 2024, We have finished work on $LaBeH_8$-like ternary hydrides and Nb-H compounds. We will promptly organize the above results into a manuscript and seek to publish this work in an appropriate journal.

For the next fiscal year, we plan to continue using the HOKUSAI supercomputer to study the high-

temperature superconductors in light element compounds at low or close to ambient pressure. We expect high-standard publications can be eventually achieved.

The specific research plan is as follows:

Recent theoretical-driven experimental observations of superconducting critical temperature $T_c > 200$ K in superhydrides gradually refocus the attention to conventional superconductors. Unfortunately, experimental realization of high-temperature superconductivity in superhydrides typically requires high pressures exceeding 150 GPa, searching for synthesizable hydrogen-rich superconductors with high-T_c at low or close to ambient pressure remains an immediate yet challenging task.

Light-element-based covalent metals were regarded as potential high-T_c superconductors because the presence of metallic covalent bonds could lead to large phonon frequencies, significant electron-phonon coupling, and high density of the states at Fermi level, which are the most critical factors for conventional superconductivity. Based on this concept, serials of high-T_c superconductor candidates were proposed, including heavily boron-doped diamond (55 K), boron-doped graphane (90 K), doped carbon clathrates (77 K), layered metal intercalated boro-carbides (> 70 K), BC_5 (45 K), and a family of SrB_3C_3 like B-C clathrate compounds (up to 79 K).

Since both boron and carbon are light atoms, the quantum lattice anharmonicity should show pronounced effects on the B-C clathrate compounds similar to the observation in superhydrides. Thus, we will re-examine the dynamical stability and superconductivity of metal-stuffed B–C clathrates ($X^{n+}[B_3C_3]^{n-}$, X can be a single metal or two metals, n denotes the average valence state) by including the quantum lattice anharmonic effects within the framework of the stochastic self-consistent harmonic approximation (SSCHA).

We will investigate quantum lattice anharmonic effects in boron-carbon sodalite-like clathrates to identify stable high-temperature superconductors under ambient and low pressure. It aims to analyze their electronic structure, lattice stability, and superconducting properties using DFT, SSCHA, and the Migdal-Eliashberg function. By evaluating anharmonic and quantum effects, the study provides a theoretical foundation for designing new superconducting materials.

6. If no job was executed, specify the reason.